Chapter 19

Challenges and Plans for Injection and Beam Dump

M. Barnes, B. Goddard, V. Mertens and J. Uythoven

CERN, TE Department, Genève 23, CH-1211, Switzerland

The injection and beam dumping systems of the LHC will need to be upgraded to comply with the requirements of operation with the HL-LHC beams. The elements of the injection system concerned are the fixed and movable absorbers which protect the LHC in case of an injection kicker error and the injection kickers themselves. The beam dumping system elements under study are the absorbers which protect the aperture in case of an asynchronous beam dump and the beam absorber block. The operational limits of these elements and the new developments in the context of the HL-LHC project are described.

1. Introduction

The beam transfer into the LHC is achieved by the two long transfer lines TI 2 and TI 8, together with the septum and injection kicker systems, plus associated machine protection systems to ensure protection of the LHC elements in case of mis-steered beam. The LHC is filled by $\sim$10 injections per beam. The MKI kicker pulse length is 8 μs, with a rise time of 0.9 μs and a fall time of 2.5 μs. Filling each ring takes 8 minutes with the SPS supplying interleaved beams to other facilities. The foreseen increase in injected intensity and brightness for the HL-LHC means that the protection functionality of the beam-intercepting devices needs upgrading. In addition the higher beam current significantly increases the beam induced power deposited in many elements, including the injection kicker magnets in the LHC ring.

The beam dumping system is also based on DC septa and fast kickers, with various beam intercepting protection devices including the beam dump block. Again, the significant change in the beam parameters for the HL-LHC implies redesign of several of the dump system devices, because of the increased energy deposition in the case of direct impact, but also because of increased radiation background which could affect the reliability of this key machine protection system.

In the following sections the function and required changes planned for the different LHC beam transfer systems are described.

2. Protection Against Injection Errors

The high injected beam intensity and energy mean that precautions must be taken against damage and quenches, by means of collimators placed close to the beam in the injection regions. The layout of the injection and associated protection devices is shown schematically in Fig. 1. The beam to be injected passes through five horizontally deflecting steel septum magnets (MSI) with a total deflection of 12 mrad, and four vertically deflecting kickers (MKI) with a nominal total kick strength of 0.85 mrad. Uncontrolled beam loss resulting from errors (missing, partial, badly synchronised or wrong kick strength) in the MKI could result in serious damage of the equipment in the LHC injection regions, in particular the superconducting separation dipole D1, the triplet quadrupole magnets near the ALICE or LHCb experiments, or in the arcs of the LHC machine itself. Damaging detector components, in particular close to the beam pipe, by excessive stray radiation is also possible.

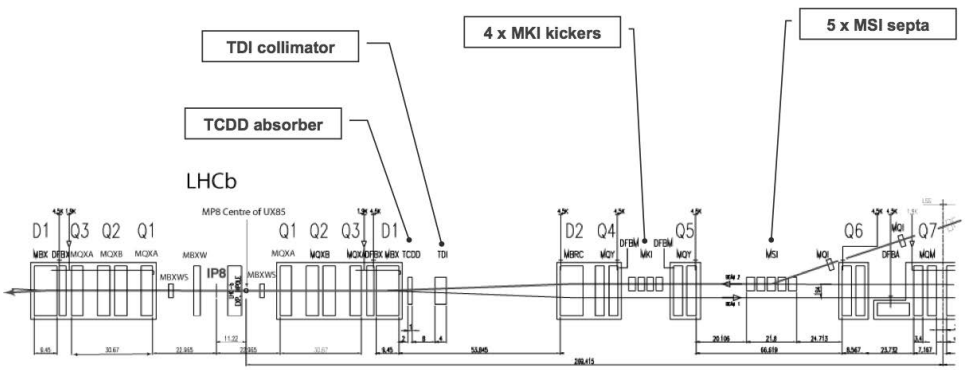

Fig. 1. Overview of injection into LHC (Beam 2, P8). The beam is injected from the right hand side.

To protect against this failure, a movable 2-sided absorber TDI is installed about 70 m from the MKI, at a 90° phase advance, in order to protect the LHC equipment. Each TDI consists of two absorber jaws. The upper jaw intercepts injected beam which is not (or not sufficiently) deflected by the injection kickers. The lower jaw intercepts the deflected circulating beam in the event of a kicker synchronisation error. Other failure scenarios have been explored in depth [3]. The most critical MKI failure is a flashover, or breakdown, in the kicker magnet which could lead to a grazing incidence beam on the TDI absorber. An accurate setup of the TDI jaws is extremely important for machine protection, in the light of the occurrence of several injection kicker failures per year with high injected intensity in LHC Run 1.

A fault on the MKI could result in the whole injected batch being mis-steered. The damage level for LHC equipment for fast and localised losses is estimated to be around 20 J/g [4]. Secondary and scattered particles must not cause damage to local equipment, in particular the D1 magnet (Fig. 1). For that purpose the TDI is complemented by a fixed mask TCDD, just in front of the D1. During such events the TDI should not itself be damaged, either in terms of the jaw material, coating, vacuum system, positioning system or in other functional ways such as integrity of the impedance shielding.

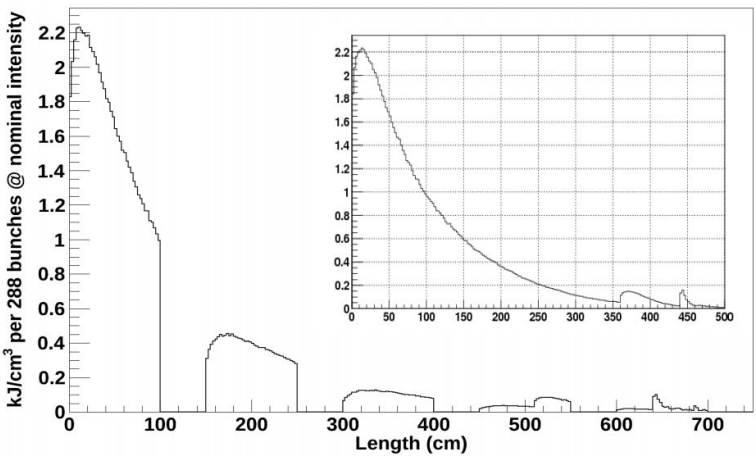

Fig. 2. Energy deposition in segmented CfC/Mo TDI absorber, with inset showing the energy deposition for the existing device.

The increased injected intensity and brightness with the HL-LHC beam parameters [1] mean that the present TDI needs redesigning, since the energy deposition and resulting thermal stresses are above the design limits of the present system. In addition, the experience from LHC Run 1 revealed several issues with the vacuum level, beam induced heating and mechanical design of the present TDI device. As a result, for HL-LHC, a completely new TDI design is being developed. The design considerations remain the same — to protect the downstream elements from damage in the event of a kicker failure — but the device concept will be revised to consist of a sequence of several shorter $\sim$1 m long collimators with jaw materials designed to survive the impact, Fig. 2, while providing enough dilution to protect the downstream D1 and triplet. In addition, the vacuum performance of the TDI needs to improve.

The TCDD masks are 1 m long Cu blocks, which in P2 are required to open for data-taking of the ALICE ZDC [2]. For the injection protection functionality a reduction of aperture of the TCDD masks is under study.

Finally, the TDI is complemented by two auxiliary collimators TCLI, which are located on the outgoing side of the triplet, at phase advances which are designed to be $\pm 20^\circ$ (modulo 180°). The present TCLIA collimators are 1.0 m long graphite jaws, based on the TCS design, and will possibly need to be replaced by more robust and more absorbing jaws. The design issues here are, besides the robustness of the TCLI jaws, the impedance heating of the two-in-one design for the TCLIA, the protection of the downstream superconducting elements and the risk of quench from injection beam losses on the TCLI jaws.

Overall, the TDI and TCLI elements need to protect the LHC arc aperture from mis-steered beams. The criteria for the protection are based on the assumed safe beam limit, which is taken as 10^{12} protons. Tracking studies showed that settings of 6.8σ for the TDI and TCLI systems adequately protect the LHC arc aperture against MKI flashovers [3]. As this depends on the injected intensity, it may be necessary to reduce the 6.8σ settings slightly for injection of higher intensity beams, which needs to be analysed in the context of the beam cleaning collimation system settings for injection.

3. Injection Kicker MKI Performances

The injection kicker (MKI) systems, at Points 2 (MKI2) and 8 (MKI8), deflect the incoming particle beams onto the accelerators equilibrium orbits. The four MKI magnets per injection are named D, C, B and A: D is the first to see injected beam. The total vertical deflection by the four MKI magnets is 0.85 mrad, requiring an integrated field strength of 1.3 Tm. Reflections and flat top ripple of the field pulse must be less than $\pm 0.5\%$, a demanding requirement, to limit the beam emittance blow-up due to injection oscillations.

Each MKI system consists of a Pulse Forming Network (PFN) and a multi-cell travelling wave kicker magnet, connected by matched transmission lines and terminated by a matched termination resistor. Each MKI magnet has 33 cells. A cell consists of a U-core ferrite sandwiched between HV conducting plates, and two ceramic capacitors sandwiched between an HV plate and a plate connected to ground (Fig. 3, right). Either 8C11 or CMD5005 ferrite is used for the MKI yoke: the data sheets for these ferrites show that the initial permeability starts to reduce for temperatures above $\sim 100\,^\circ$C.

After an MKI magnet is installed in a vacuum tank (Fig. 3, left), and prior to mounting vacuum valves, the complete magnet is baked out, in an oven, to $300\,^\circ$C for at least 48 hours: the bake-out permits the MKIs to achieve a vacuum of around 10^{-11} mbar. Following cool-down the MKI is HV pre-conditioned to a PFN voltage of 56.6 kV. Subsequently the MKI is returned to the clean-room, vacuum valve actuators are installed, and bake-out jackets are mounted on each vacuum

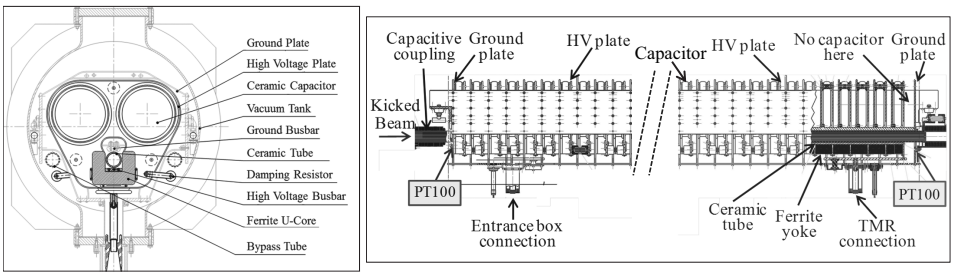

Fig. 3. MKI kicker magnet.

tank. The jackets are used to re-bake the MKI before a final HV conditioning. The jackets remain on the tank such that a bake-out of the MKI can be carried out in the LHC tunnel, if required.

The 3414 mm long, 540 mm diameter, tanks housing the MKI magnets are reused from the LEP accelerator: they were used for 300 kV electrostatic separators and thus were electro-polished. Each vacuum tank requires a bypass tube for the counter-rotating beam: high conductivity copper is used. Figure 3 shows two bypass tubes — this allows an MKI to be used at either LHC injection point. Small longitudinal slots, in the copper, connect the vacuum of the tank and the bypass tube.

A number of effects have been observed for the MKI magnets during operation in the LHC: these include beam induced heating of the ferrite yoke, inefficient cooling of the ferrite yoke, occasional beam induced heating of ferrite toroids outside of the magnet yoke, electrical flashovers, unidentified falling objects (UFOs) and electron-cloud [6].

3.1. *Beam induced heating of ferrite yoke*

A beam screen (electromagnetic shield) is placed in the injected beam aperture of each magnet, to provide a path for the image current of the LHC beam and screen the ferrite yoke against wake fields. The screen consists of a ceramic tube with conductors lodged in grooves in the inner wall. To limit longitudinal beam coupling impedance, while allowing a fast magnetic field rise-time, the conductors are connected to the standard LHC vacuum chamber at one end and are capacitively coupled to it at the other end [7]. In the original design the extruded ceramic tube had 24 nickel-chrome (80/20) conductors, each 0.7 mm $\times$ 2.7 mm with rounded corners, inserted into slots. In the version installed in the LHC prior to the 2013–2014 long shutdown one (LS1), nine conductors closest to the HV busbar were removed to reduce the maximum electric field. This beam screen ensured a low rate of flashover on the inner surface of the ceramic tube and, initially, an adequately

low beam coupling impedance. However with high LHC beam currents, integrated over the several hours of a good physics fill, the real component of beam coupling impedance of the magnet ferrite yoke can lead to significant beam induced heating.

When the temperature of the MKI ferrite yoke approaches the Curie point the strength of the kick reduces and the mis-kicked injected beam could result in quenches of several superconducting magnets. Hence there is an interlock to inhibit injection if the measured yoke temperature is above specified thresholds. As a result of low emissivity of the inside of the MKI vacuum tanks the time-constants for the measured ferrite cool-down are relatively long: on about ten occasions, during 2012, after a series of long fills, it was required to wait longer than one hour before injecting to allow the cool-down of the MKI8D yoke, thus limiting the running efficiency of the LHC.

Extensive simulations have been carried out to understand the cause of, and to significantly reduce, the beam induced heating: the beam screen implemented during LS1 (2013–2014) will have a full complement of 24 screen conductors [8]. The cause of heating of the hottest MKI magnet, during 2012, has been identified to be caused by a non-conformity of the ceramic tube, leaving part of the ferrite yoke unscreened: this led to about double the power deposition. Going from 15 to 24 screen conductors would have reduced the power deposition by a factor of 4, relative to a conforming ceramic tube, for pre-LS1 beam conditions (50 ns bunch spacing, 1.2 ns 4σ bunch length, 1380 bunches and 1.6×10^{11} ppb). For post LS1 beam conditions (25 ns bunch spacing, 1.0 ns 4σ bunch length, 2808 bunches and 1.15×10^{11} ppb) the change from 15 to 24 screen conductors even lead to a reduction of beam induced power by a factor seven, due to the difference in the beam power spectrum.

The HL-LHC beam option with 50 ns bunch spacing and 3.5×10^{11} ppb leads to the highest power deposition in the MKI magnets up to 240 W/m [9], always assuming 24 screen conductors. This is significantly more than the power deposited in the magnet yoke associated with the non-conform ceramic tube which was installed pre-LS1, estimated to be 160 W/m and leading to temperatures which limited operation. For 25 ns bunch spacing and 2.5×10^{11} ppb the expected deposited power has been calculated to be between 125 W/m and 190 W/m. Thus, in addition to the increased number of screen conductors, the cooling of the ferrite yoke is studied as an additional measure.

3.2. *Cooling of ferrite yoke*

The MKI magnet is operated in a vacuum of $\sim 10^{-11}$ mbar thus convection does not contribute to cooling of the ferrite yoke. In addition, many of the materials used in the kicker magnet have relatively poor thermal conductivity hence cooling

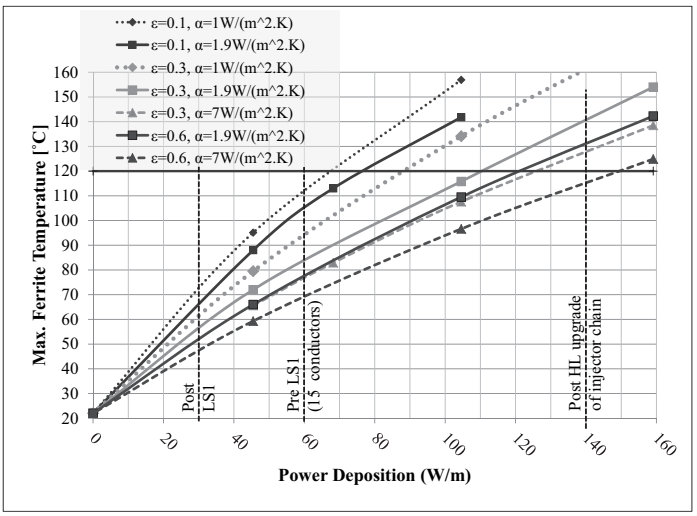

Fig. 4. Predicted steady-state ferrite temperature versus total power deposition per meter length of ferrite yoke, for various emissivities of the inside of the MKI tank and convection (α). 15 and 24 straight screen conductors are considered for pre and post LS1, respectively.

is mainly due to thermal radiation. Thermal simulations, confirmed by measurements, show that the inside of an electropolished MKI tank has an emissivity (ϵ) of $\sim$0.1. Such a low emissivity results in a relatively high steady-state temperature of the ferrite yoke. Thermal simulations predict that the steady-state yoke temperature is proportional to $\epsilon^{-0.16}$. In addition transient thermal simulations predict that the time constant for cool-down of the ferrite yoke, in hours, is given by $(10/\sqrt{\epsilon})$ [10]. Thus an increased emissivity has the benefit of both reducing the maximum ferrite temperature and the cool-down time-constant.

Figure 4 shows a plot of predicted ferrite temperature versus total power deposition per metre length of ferrite yoke, for various emissivities of the tank and heat transfer coefficients by convection (α). A standard bake-out jacket for an MKI has an α in the range 1.9–2.9 W/(m^{2}K). An MKI without a bake-out jacket is represented by $\alpha = 7$ W/(m^{2}K). Figure 4 shows that for ϵ of 0.1 the expected ferrite temperature will be well below the Curie temperature for beam parameters to be used after LS1, but not for HL-upgrade parameters. A tank emissivity of at least 0.6, without bake-out jackets, is required to maintain the ferrite yoke temperature below 120 °C. Water cooling of the outside of the vacuum tank is studied to reduce the ferrite temperature. In addition water cooling of the internal side plates, which are nominally at ground potential, is being considered.

The pre-treatment of the MKI vacuum tanks by an ion bombardment technique, in an atmosphere of argon and oxygen [10] is being studied during LS1. Results

are not conclusive at the moment and other means of increasing the emissivity of the inside of the tank are being studied.

3.3. *Ferrite toroid heating*

There has also been occasional unexpected heating of some toroidal ferrites, nine of which are mounted at each end of the ceramic tube, whose purpose is to damp low-frequency resonances. Each set of nine toroids has two types of Ferroxcube NiZn ferrite, namely 4M2 and 4B3, with a Curie point of 200 °C and 250 °C, respectively. One set of nine toroids, at the capacitively coupled end of the beam screen occasionally reached 193 °C measured; all others remained below 100 °C measured. The source of the heating is still under investigation.

3.4. *Surface flashover of ceramic tube*

A voltage is induced on the screen conductors, mainly by mutual coupling with the MKI magnet cell inductance. Hence the voltages, at the open end of the screen conductors, show a positive peak (max.) during field rise and a negative peak during field fall: the height of the maximum is about twice the magnitude of the minimum. Figure 5 shows the predicted maximum voltage versus conductor number. The predicted maximum voltage between adjacent screen conductors is also shown, the highest value is ∼2.7 kV.

Extensive 3D electromagnetic simulations have been carried out to study electric fields on the surface of the ceramic tube. The predictions show that, as a result of the high permittivity (10) of the alumina, equipotential lines penetrate into the ceramic between adjacent screen conductors. The predictions, for 15 and 19 conductor versions, together with previous observations of the surface flashover

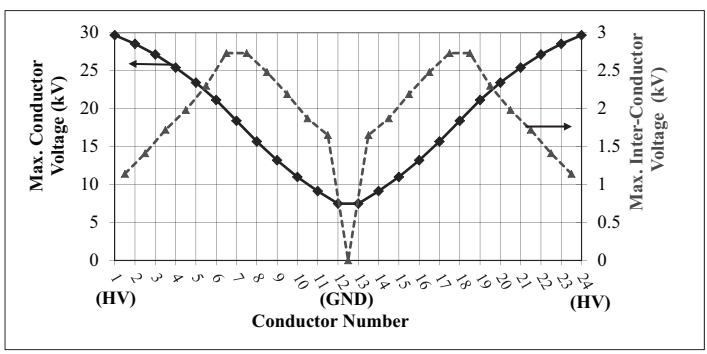

Fig. 5. Conductor (solid) and inter-conductor (dashed) voltages, for 24 screen conductors, for 60 kV PFN voltage.

inception voltage, have been used to determine the upper limit for the predicted electric field (∼12 kV/mm). Removing some metallisation and replacing it with an offset cylinder, reduces the maximum electric field by a factor of more than 2, providing a safety margin for operation at the PFN design voltage of 60 kV. Tests in the laboratory, with all screen conductors pulsed to the same voltage, confirm the aforementioned predictions.

3.5. *Electron cloud*

Prior to LS1 significant pressure rises, due to electron-cloud, occurred in and nearby the MKIs: the predominant gas desorbed from surfaces is H_2. A pressure rise also increases the number of unidentified falling objects (UFOs) [11] and may augment the probability of electrical breakdown in the magnet and surface flashover on the ceramic tube. Conditioning of surfaces reduces electron-cloud, and thus pressure rise, but further conditioning is often required when beam parameters (e.g. bunch spacing, bunch length and bunch intensity) are pushed.

The ceramic tube of an MKI magnet replaced during Technical Stop 3 (TS3) in September 2012 had a high secondary electron yield when installed and required conditioning with beam, together with metallic surfaces facing the beam (e.g. screen conductors): Fig. 6 shows pressure, measured both in the upgraded MKI8D tank and nearby interconnects, normalized to the number of protons (p). The highest normalized pressure occurred in interconnect MKI8D-Q5, followed by interconnect MKI8C-MKI8D. Initially the beam current was kept low to maintain

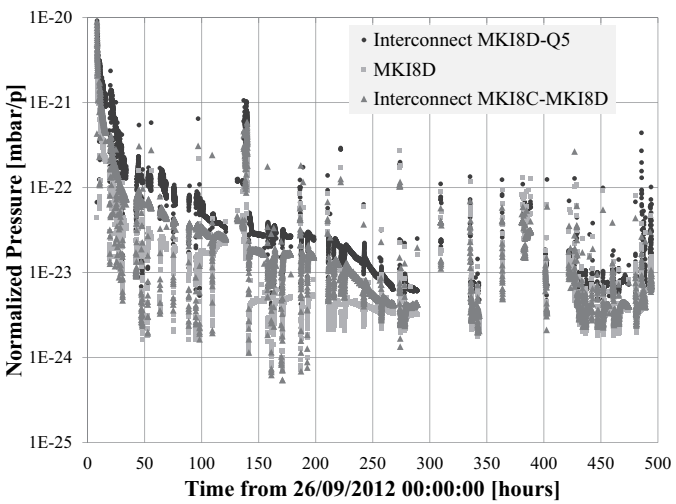

Fig. 6. Pressure after TS3, measured both in and nearby tank MKI8D, normalized to the number of protons.

the pressure below the interlock thresholds. The ceramic tube conditioned relatively quickly but required 250 hours, with beam, to achieve a normalized pressure similar to the pre-replacement ($\sim 4\times10^{-24}$ mbar/p) level.

In order to mitigate electron multipacting the MKI interconnects and bypass tubes (Fig. 3) have been NEG coated during LS1. The adjacent beam instrumention (BTVSI and BPTX) have also been NEG coated during LS1. In addition NEG cartridges have been installed, on the cold-warm transition, to supplement existing ion pumps. On the MKI interconnects the ion pump has been exchanged for a version which also includes a NEG cartridge.

3.6. *Fast transient beamlosses (UFOs)*

There have been a total 21 protective beam dumps due to fast transient beamlosses (termed UFOs) at the MKIs. This is about half the number of UFO related beam dumps which occurred in the LHC. The UFO activity around the injection kicker in P2 generally exceeded that around the MKI8s [11]. After a comprehensive study program in 2011, the MKI UFOs were identified as macro particles originating from the ceramic tube inside the MKI magnets [14]. Thus the MKI8D installed during TS3 had improved cleaning of the ceramic tube, which included iterations of flushing of the inside of the tube with N_2 at 10 bar and dust sampling, until no significant further reduction of macro particles was noted. Before TS3, MKI8D had the highest UFO activity of the MKIs in P8; the replacement MKI8D had the lowest UFO activity [11]. Extensive additional cleaning has been carried out on the ceramic tubes which have been put in place during LS1.

With 15 screen conductors installed, macro particles could be detached from the inside of the ceramic tube and accelerated towards the beam by the high electric field when the kicker is pulsed [14]. The 24 screen conductors reduce the electrical field during most of the MKI pulse hence decreasing the probability of a particle being detached from the ceramic.

3.7. *Possible future upgrades and ongoing R&D*

Ferrite such as CMD10, which has a higher Curie temperature than the CMD5005 or 8C11 presently used for the MKI yoke, would permit high-intensity beam operation with better availability. However, operating at higher yoke temperatures will result in higher pressure in the vacuum tank which may result in an increased electrical breakdown and surface flashover rate [15].

As mentioned above, as a result of multipacting in the copper bypass tube, significant pressure rise can occur in an MKI tank, hence the copper bypass tubes have been NEG coated during LS1. However, if the counter-rotating beam still has

a detrimental effect upon the MKI operation, the vacuum of the bypass tube could be separated from the vacuum of the MKI tank.

A series of high voltage tests are planned for the laboratory in which different gases are injected into a test tank: this will allow a careful and systematic study of the effect of gas pressure upon surface flashover of the ceramic tube. These studies will permit the MKI vacuum interlock thresholds to be optimized and the possibility, from the MKI vacuum perspective, of using a higher Curie temperature ferrite to be evaluated.

4. Beam Loss Control at Injection

Losses at injection into the superconducting LHC can adversely affect the collider performance in several important ways. Injection related losses can produce spurious signals on the sensitive beam loss monitoring system which will trigger beam dumps. In addition, the use of the two injection insertions to house downstream high energy physics experiments brings constraints on permitted beam loss levels, to avoid trips or even damage to the sensitive detector sub-assemblies.

The apertures in the injection region are small, in particular at the MSI septum and the MKI kicker, to be able to achieve the required deflections with achievable septum and kicker currents and to minimise the stray field in the field free septum holes. The physical radius of the protective mask immediately upstream of the MSI is 10 mm, from which orbit and alignment tolerances need to be subtracted. For the circulating beam the MSI provides 7.3σ aperture in n1 notation [16]. The MKI has a ceramic chamber with 39 mm ID. For HL-LHC beams the energy in each injected batch will increase to $\sim$4.5 MJ, which is about a factor 25 above that required to damage accelerator components in the event of direct impact. To protect the small apertures in the injection regions, and also to prevent injection into the LHC of beams with large oscillations, protection devices TCDI are set around the injected beam trajectory in the transfer lines TI 2 and TI 8. There are three devices per plane, spaced at 60 degrees in betatron phases, Fig. 7, with settings of $\pm 4.5\sigma$. The TCDIs are two-jawed movable devices, with 1.2 m of Carbon to intercept the beam.

The beam loss monitoring BLM system for the LHC ring is designed to protect the machine against quenches and damage from beam loss. The location near the superconducting elements in the LHC tunnel of some of the TCDI protection devices, together with the TDI and TCLIs, means that there is very strong cross-talk between injection losses and the beam loss signals from circulating beam. Although the loss limits are well below quench levels, for beams with large transverse tails, large emittance or poor trajectories, the BLMs can frequently trigger, resulting in a beam abort and reducing machine availability.

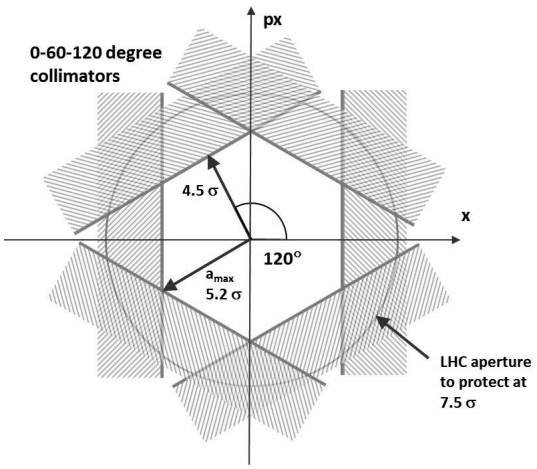

Fig. 7. Phase space coverage of TCDI collimators in TI 2 and TI 8 transfer lines, courtesy V. Kain.

The nominal emittance for the LHC beam transfer and injection is 3.5 mm mrad, normalized emittance. The emittances injected into the LHC in the years 2010 to 2012 were slowly reduced from about 3.0 mm mrad to below 2.0 mm mrad, the latter made possible by the change to double-batch injection with the 50 ns beam. Despite this reduction in emittance, the increasing beam intensity and push for better availability meant that many mitigations against beam loss in the injection regions were deployed through Run 1. First was an increase in the thresholds of the LHC BLMs. Then local shielding was added between the critical TCDIs and the LHC elements, optimized after a series of FLUKA simulations. The reduction factor in beam loss per proton at the affected BLMs was expected to be a factor of 3, and was measured to be slightly less, at around a factor of 2–2.5 depending on location.

The key factor for losses on TCDIs are scraping of tails in the SPS, which has been shown to provide a factor of $\sim$10 reduction [17]. The same studies also demonstrated that injection of 3.5 mm mrad emittance beams is possible with similar loss levels to 2 mm mrad, an important result for future LHC operation and HL-LHC parameters.

In addition to the beam size and tails, trajectory instability in the transfer lines can increase losses on TCDIs. The stability of the lines has been analyzed in detail [18] and is the subject of ongoing studies. The main source of errors are shot-to-shot variations in the horizontal plane, likely due to variations in the field of the extraction septa in the SPS. The lines need correcting about once per week in order to keep the trajectories within the allocated tolerances, which gives enough operational margin for injection beam losses. Importantly, this is sufficient to run with-

out repeated setup of the TCDI collimators, despite their close settings of $\pm 4.5\sigma$, and it was possible to run a full year without setting up the TCDIs again. For the future an automated procedure is being considered.

In the LHC, uncaptured circulating beam leads to beam loss on the TDI and TCLIs when the injection kicker pulses, with high loss rates recorded on the TCTVBs (which are not part of the injection protection system); this was a major problem in 2010 operation and was the subject of several mitigation measures. The first mitigation was to increase BLM thresholds to avoid dumping, especially on TCTVB collimators. FLUKA simulations were performed to understand energy deposition and to optimize shielding design. The RF capture voltage in the LHC was increased, and finally the use in regular operation of a gated excitation of the transverse damper was deployed for both abort gap cleaning AGC [19] and injection gap cleaning IGC [20]. In these modes the damper excitation is gated such as to clean away uncaptured beam which would otherwise drift around the ring and be swept onto the TDI by the MKI pulse. The combination of AGC and IGC is very effective, and reduces the beam loss of uncaptured beam on the TDI by a factor of ~ 10.

For the HL-LHC era, the foreseen improvements to overcome injection losses are to remove the most troublesome TCDI collimators from the LHC tunnel, to new locations in the transfer line with suitable phase and betas. The scraping in the SPS and the stability of the transfer lines are also areas where improvements are being studied. For the uncaptured beam, the AGC and IGC functionality will need to be maintained and possibly improved. Further developments on the beam loss measurement system are ongoing to cope with injection losses. Smaller ionization chambers have been developed, which have a larger dynamic range than the standard beam loss monitors used across the LHC and avoid saturation during injection. A second development is to temporarily disable the interlocking ability of a selected set of beam loss monitors in the injection region, for some ms at the moment of injection [21].

5. Beam Dump System Performance Reach

The beam in the LHC is aborted or dumped by a dedicated system based on pulsed extraction kickers and DC septum magnets located in the dedicated insertion in Point 6 (P6), followed by a dilution kicker system MKB, long drift chamber and graphite beam dump absorber block TDE, kept at atmospheric pressure of N_2. The 3 μs rise time of the kicker field is synchronized by a highly reliable timing system [24] to a beam-free abort gap in the circulating bunch pattern. The horizontal and vertical dilution kickers are powered with anti-phase sinusoidal currents so as to paint the bunches onto the TBE with an elliptical shape, Fig. 8.

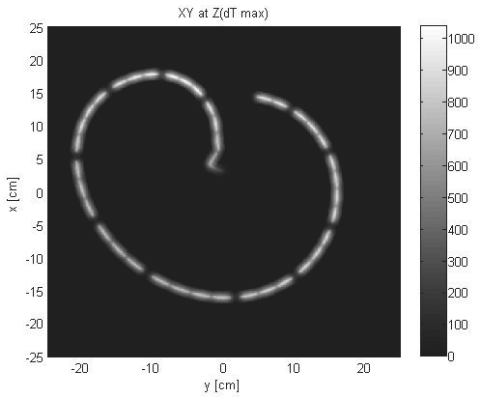

Fig. 8. Sweep form of 25 ns spacing LHC beam on TDE dump block, with 1.7×10^{11} p+ per bunch.

Various instruments are also used to set up and monitor the quality of the beam dump action, and comprehensive internal and external quality checks are made using sophisticated pattern recognition algorithms after each dump action to verify the dump quality, both in terms of losses and trajectory and in terms of hardware performance and detection of any failures in redundant pathways. The dump system is designed to have a very high reliability, SIL4, which corresponds to an expected beyond-design failure rate of fewer than once per 10,000 years [25].

The beam dump block TDE is designed to withstand the impact of the so-called 'ultimate' LHC beam, which contains 2808 bunches of 1.7×10^{11} protons at 25 ns spacing, with acceptable thermal stresses in the TDE core [26]. The peak energy deposition and temperature rise depend on the details of the sweep shape. With the present sweep the maximum temperature increase with the HL-LHC beam increases from 1000 to 1350 °C, Fig. 9. It remains to be seen whether this is still acceptable in terms of the TDE robustness — further simulations are needed, and possibly test in the HiRatMat beam facility can be used to confirm the models used.

In case the TDE temperature rise after the impact of the HL-LHC beam is not acceptable, possible solutions could be to replace the TDE cores with new blocks, with lower density and higher robustness carbon fibre composite, or to modify the MKB dilution kicker system to increase the sweep frequency by about 50%. Both approaches need more detailed study.

Another concern will be the total energy deposited in the dump blocks, which have a thermal time constant of about 4.5 hours and reached a maximum temperature of about 20 °C above ambient during 2012, when the maximum dumped energy was 140 MJ, a factor of 5 lower than the 690 MJ for HL-LHC. The block cooling and N_2 gas handling may also need upgrading to cope with the increase in the average and peak beam power.

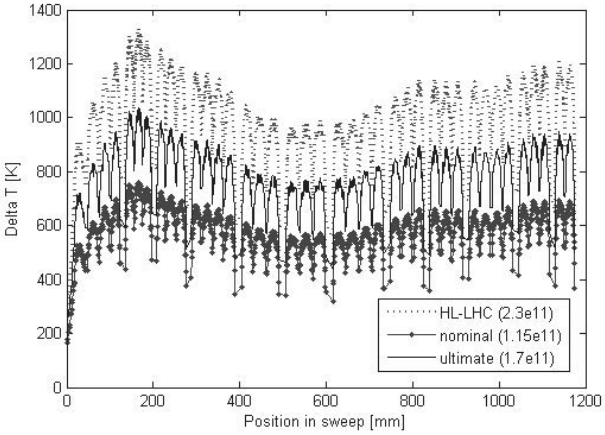

Fig. 9. Temperature rise at shower maximum in the TDE dump block, as a function of position along the sweep length, for different 25 ns beams.

6. Protection Against Beam Dumping Errors

Several failure modes exist in the synchronization system and in the kicker switches which could lead to an asynchronous dump, in which the full beam intensity would be swept across the LHC aperture by the rising kicker field. Without dedicated protection devices this would lead to massive damage of the LHC magnets in LSS6 and the downstream arcs 5-6 and 6-7, and depending on the operational configuration a number of collimators and possibly experimental triplet magnets.

A large amount of redundancy and fault tolerance has been built into the LHC dump system to avoid producing these asynchronous dumps; nevertheless, during Run 1, two such events happened, although without beam loss as one was at injection energy with a single pilot bunch and the second event occurred without beam. To avoid the machine damage, a series of passive protection devices have been designed to intercept the swept particles. The first such element TCDS is a fixed absorber block located directly in front of the extraction septum, which intercepts about 50 bunches at 25 ns spacing. The second system is the TCDQ which is located just upstream of the next superconducting quadrupole Q4, and this is a movable device which has to be adjusted as a function of beam size and orbit. It intercepts about 30 bunches, and is complemented by a two-sided collimator TCSG set $\sim 0.5\sigma$ closer to the beam and a 2 m long fixed mask TCDQM which is slightly smaller than the aperture of the Q4.

The increased beam intensity and brightness for HL-LHC will require a redesign of the TCDS and TCDQ absorbers. The TCDQ re-design has been analyzed in detail [27] and the new design will already be installed for LHC Run 2.

This extends the absorber length from 6 to 9 m, and replaces the higher density graphite absorber material by different densities (1.4 and 1.8 g/cm^3) of carbon fibre composite (CfC). The energy deposition and induced thermal stresses then remain acceptable [22] during an asynchronous abort, Fig. 10, and the protection of Q4 and downstream elements remains sufficient with energy deposition in the magnet coils of around 20 J/cm^3 [23]. Operational experience and further simulations will show if it will be necessary to improve the TCDQ positioning accuracy, which is presently around 50 μm. If required, changes of the electronics and control system but also of the mechanical system of the TCDQ need to be foreseen.

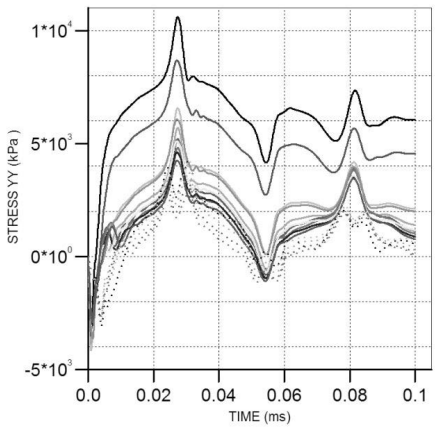

Fig. 10. Time evolution of vertical (YY) stresses in the new CfC TCDQ block for an asynchronous dump with HL-LHC beam, courtesy T. Antonakakis.

A similar level of redesign will be needed for TCDS. Here any additional length will reduce slightly the aperture for the circulating or extracted beams, by a small fraction of a sigma, which should be acceptable. The TCSG collimators will be upgraded with integrated button BPMs in the jaws, which should allow faster and more accurate setup.

7. Beam Dump Kicker Performance Upgrades

The spontaneous triggering of the LHC beam dumping system switches, resulting in a dump asynchronous to the abort gap, cannot completely be avoided. The expected rate of asynchronous dumps is about one per beam dumping system per year. Asynchronous beam dumps have a negative effect on the machine availability, as one can expect the quench of a number of magnets in case that the asynchronous dump occurs at full beam energy during a normal physics run. The asynchronous beam dump also puts a strain on the protection elements described

above, as their correct positioning must be guaranteed to avoid damage to machine elements at the moment of an asynchronous beam dump.

One of the sources of spontaneous triggering of the beam dump kicker is the Single Event Burnout (SEB) of the Fast High Current Thyristor (FHCT) switches when exposed to radiation. The SEB failure rate depends primarily on the voltage over the switch, which in the case of the LHC beam dumping system is tracking the beam energy, the energy of the radiation to which the switch is exposed and its charge. Measurements of the effect of radiation on the MKD and MKB FHCT switches have been performed at the H4IRRAD irradiation facility [28]. As a result the switches of some of the MKD generators are exchanged during LS1 so all switches installed will be of the one manufacturer which showed a significantly lower SEB during the tests. The shielding of the cable ducts between the generators and the LHC tunnel is also improved during LS1. When operation at almost double the beam energy will start in 2015 the performance of the system in the light of erratic triggering due to radiation will need to be closely surveyed. If necessary, further shielding against radiation will be required.

To follow the recommendations of the FHCT switch manufacturer it is foreseen to increase the power trigger dI/dt from the present 400 A/μs to 1 kA/μs and increase the switching trigger peak current from 400 A to about 800 A. This requires the upgrade of the trigger transformer system which is presently under development. At the same time the IGBT switches of the power triggers have already been upgraded during LS1 to allow for an increased trigger voltages and the larger dI/dt. These changes have the aim to increase the switch lifetime. The end of lifetime is expected to manifest itself by an increased leakage current which will result in an internally triggered synchronous beam dump. However, it is also possible that at the end of the lifetime of a switch the likelihood of erratic triggering increases, which will lead to asynchronous beam dumps. The expected lifetime of a switch is around 1 million pulses. With approximately 20,000 pulses per system per year, a large scale exchange of the FHCT switches during the HL-LHC era should normally not be required. The same applies to the capacitors used in the pulse generators.

Other possible changes of the generators include the addition of saturable cores at the top of the FHCT stack. The cores are foreseen to avoid resonances in the generator at the moment of switching and by this reduce the spark rate between the switch and the insulators of the generators. The saturable cores can at the same time give a gain in rise time, which is very favourable. Operation at full voltage of the MKD generators with the newly inserted insulators during LS1 will need to be carefully monitored.

The delay between the erratic switching of one power switch and the re-triggering of the complete beam dumping system (the asynchronous dump) is

presently around 800 ns. If this delay is proven to be critical, based on operational experience and simulations, the delay can possibly be shortened. This will require the development of new electronic systems.

Acknowledgments

All systems described in this chapter have been designed, built, commissioned and successfully operated as a result of the diligent work and efforts of many colleagues and collaborators from various groups, who are far too numerous to mention individually. We thank them all.

References

[1] G. Rumolo, HL-LHC beam parameters, CERN EDMS document 1296306, https://edms.cern.ch/document/1296306/1.
[2] ALICE Collaboration, The Zero Degree Calorimeters for the ALICE Experiment, CERN-ALICE-PUB-99-17, 1999.
[3] V. Kain *et al.*, The expected performance of the LHC injection protection system, presented at EPAC'04; 9th European Particle Accelerator Conference 2004.
[4] O. Brüning and J. B. Jeanneret, Optics constrains imposed by the injection in IR2 and IR8, CERN/LHC Project Note 141 1998.
[5] LHC Design Report, http://ab-div.web.cern.ch/ab-div/Publications/LHC-Design Report.html.
[6] M. J. Barnes *et al.*, Upgrade of the LHC Injection Kicker Magnets, in *Proc. of IPAC'13*, MOPWA030; http://www.JACoW.org.
[7] M. J. Barnes, F. Caspers, L. Ducimetiére, N. Garrel and T. Kroyer, The Beam Screen for the LHC Injection Kicker Magnets, in *Proc. EPAC'06*, TUPLS011; http://www.JACoW.org.
[8] H. Day, Measurements and Simulations of Impedance Reduction Techniques in Particle Accelerators, CERN-THESIS-2013-083.
[9] H. Day *et al.*, Beam Coupling Impedance of the New Beam Screen of the LHC Injection Kicker Magnets, in *Proc. IPAC'14*, TUPR1030; http://www.JACoW.org.
[10] M. J. Barnes *et al.*, Beam Induced Ferrite Heating of the LHC Injection Kickers and Proposals for Improved Cooling, in *Proc. IPAC'13*, MOPWA031; http://www.JACoW.org.
[11] T. Baer *et al.*, UFOs: Observations, Statistics and Extrapolations, in *Proc. LHC Beam Operation Workshop*, Evian, 17–20 December 2012.
[12] G. Rumolo and G. Iadarola, private communication, 16 April 2013.
[13] T. S. Sudarshan and J. D. Cross, *The Effect of Chromium Oxide Coatings on Surface Flashover of Alumina Spacers in Vacuum*, IEEE Trans. on Electrical Insulation, Vol. EI-11, No. 1, March 1976, pp. 32–35.
[14] B. Goddard *et al.*, Transient Beam Losses in the LHC Injection Kickers from Micron Scale Dust Particles, in *Proc. IPAC'12*, TUPPR092; http://www.JACoW.org.

[15] M. J. Barnes, L. Ducimetiére, N. Garrel, B. Goddard, V. Mertens and W. Weterings, Analysis of Ferrite Heating of the LHC Injection Kickers and Proposals for Future Reduction of Temperature, in *Proc. IPAC'12*, TUPPR090; http://www.JACoW.org.
[16] J. B. Jeanneret and R. Ostojic, Geometrical acceptance in LHC version 5.0, CERN-LHC-Note-111, 1997.
[17] B. Goddard *et al.*, Beamloss Control at Injection into the LHC, CERN-ATS-2011-274, 2011.
[18] L. Drosdal *et al.*, Analysis of LHC Transfer Line Trajectory Drifts, in *Proc. IPAC'13*, MOPWO033; http://www.JACoW.org.
[19] W. Bartmann *et al.*, LHC abort gap cleaning studies during luminosity operation, in *Proc. IPAC'12*, MOPPD058; http://www.JACoW.org.
[20] A. Boccardi *et al.*, Summary of Injection pre-cleaning tests performed on October 27, 2010, CERN-ATS-Note-2010-050 PERF. 2010.
[21] C. Bracco *et al.*, Injection and lessons for 2012, in *Proc. Chamonix 2012 Workshop on LHC Performance*, pp. 65–68.
[22] T. Antonakakis and C. Maglioni, Upgrade of the TCDQ: A dumping protection system for the LHC, sLHC Project Note 0041, 2013.
[23] R. Versaci, B. Goddard and V. Vlachoudis, LHC Asynchronous Beam Dump: Study of new TCDQ model and effects on downstream magnets, CERN-ATS-Note-2012-084 MD, 2012.
[24] A. Antoine, E. Carlier and N. Voumard, The LHC Beam Dumping System Trigger Synchronisation and Distribution System, *ICALEPCS2005*, Geneva, 2005.
[25] R. Filippini, Dependability analysis of a safety critical system: the LHC beam dumping system at CERN, CERN-THESIS-2006-054 - Pisa U., 2006.
[26] J. Zazula and S. Péraire, LHC beam dump design study; 1, simulation of energy deposition by particle cascades; implications for the dump core and beam sweeping system, CERN-LHC-Project-Report-80, 1996.
[27] R. Versaci, B. Goddard and V. Vlachoudis, LHC Asynchronous Beam Dump: Study of new TCDQ model and effects on downstream magnets, CERN-ATS-Note-2012-084 MD, 2012.
[28] V. Senaj and L. Ducimetiére, Attempt to a non-destructive single event burnout test of high current thryristors, in *Pulsed Power Conference, 2011 IEEE* (IEEE, 2011), pp. 797–796.